

# 1 Clustering diurnal cycles of day-to-day temperature change to 2 understand their impacts on air quality forecasting in mountain- 3 basin areas

4 Debing Kong<sup>1,2</sup>, Guicai Ning<sup>3,4\*</sup>, Shigong Wang<sup>3,5</sup>, Jing Cong<sup>6</sup>, Ming Luo<sup>5,7</sup>, Xiang Ni<sup>1,2</sup>, Mingguo  
5 Ma<sup>1,2</sup>

6 <sup>1</sup>Chongqing Jinpo Mountain Karst Ecosystem National Observation and Research Station, School of Geographical  
7 Sciences, Southwest University, Chongqing, 400715, China

8 <sup>2</sup>Chongqing Engineering Research Center for Remote Sensing Big Data Application, School of Geographical Sciences,  
9 Southwest University, Chongqing, 400715, China

10 <sup>3</sup>The Gansu Key Laboratory of Arid Climate Change and Reducing Disaster, College of Atmospheric Sciences, Lanzhou  
11 University, Lanzhou 730000, China

12 <sup>4</sup>Institute of Environment, Energy and Sustainability, The Chinese University of Hong Kong, Shatin, N.T., Hong Kong,  
13 China

14 <sup>5</sup>Sichuan Key Laboratory for Plateau Atmosphere and Environment, School of Atmospheric Sciences, Chengdu University  
15 of Information Technology, Chengdu 610225, China

16 <sup>6</sup>Tianjin Municipal Meteorological Observatory, Tianjin 300074, China

17 <sup>7</sup>School of Geography and Planning, and Guangdong Key Laboratory for Urbanization and Geo-simulation, Sun Yat-sen  
18 University, Guangzhou 510275, China

19 \*Correspondence to: Dr. Guicai Ning ([ninggc09@lzu.edu.cn](mailto:ninggc09@lzu.edu.cn))

20 **Abstract.** Air pollution is substantially modulated by meteorological conditions, and especially their diurnal variations may  
21 play a key role in air quality evolution. However, the behaviors of temperature diurnal cycles along with the associated  
22 atmospheric condition and their effects on air quality in China remain poorly understood. Here, for the first time, we  
23 examine the diurnal cycles of day-to-day temperature change and reveal their impacts on winter air quality forecasting in  
24 mountain-basin areas. Three different diurnal cycles of the preceding day-to-day temperature change are identified and  
25 exhibit notably distinct effects on the day-to-day changes in atmospheric dispersion conditions and air quality. The diurnal  
26 cycle with increasing temperature obviously enhances the atmospheric stability in the lower troposphere and suppresses the  
27 development of the planetary boundary layer, thus deteriorating the air quality on the following day. By contrast, the diurnal  
28 cycle with decreasing temperature in the morning is accompanied by a worse dispersion condition with more stable  
29 atmosphere stratification and weaker surface wind speed, thereby substantially worsening the air quality. Conversely, the  
30 diurnal cycle with decreasing temperature in the afternoon seems to improve air quality on the following day by enhancing  
31 the atmospheric dispersion conditions on the following day. The findings reported here are critical to improve the  
32 understanding of air pollution in mountain-basin areas and exhibit promising potential for air quality forecasting.

33

## 34 1. Introduction

35 Air pollution is not only affected by anthropogenic emissions (Streets et al., 2001; Zhang et al., 2009; Kelly and Zhu, 2016),  
36 but also controlled by atmospheric dispersion conditions (Wei et al., 2011; Li et al., 2015; Ye et al., 2016; Zhang et al.,  
37 2020). Stagnant meteorological conditions significantly contribute to the formation and maintenance of heavy air pollution  
38 as they play important roles in regulating the increment of air pollutants concentrations (Deng et al., 2014; Bei et al., 2016;  
39 Zhang et al., 2016; Wang et al., 2018). It is noted that atmospheric dispersion capacity is substantially modulated by synoptic  
40 patterns and hence the evolutions of large-scale synoptic systems can lead to the improvement or deterioration of air quality  
41 (Yarnal, 1993; Miao et al., 2017; Ning et al., 2019; Dong et al., 2020; Ning et al., 2020). In China, high anthropogenic  
42 emissions from coal-fired heating (Xiao et al., 2015), frequent temperature inversion (Xu et al., 2019; Feng et al., 2020; Guo  
43 et al., 2020), and shallow planetary boundary layer (PBL) structure (Li et al., 2017; Miao et al., 2018; Su et al., 2020) result  
44 in frequent occurrence of heavy air pollution events in winter. These factors highlight the significance of further revealing  
45 the physical mechanism of atmospheric dispersion evolutions.

46  
47 The behaviors of diurnal cycles of atmospheric dispersion conditions and their effects on air quality remain poorly  
48 understood although air pollution significantly modulated by atmospheric dispersion conditions has been well demonstrated.  
49 For instance, as a typical synoptic process occurring in winter in China, the cooling process could cause rapid changes in  
50 meteorological and environmental conditions. Cooling processes induce significant day-to-day temperature variations and  
51 thus result in substantial changes in air quality (Hu et al., 2018; Ning et al., 2018b; Kang et al., 2019). Many previous studies  
52 revealed that cooling processes could remove air pollutants by invading lots of cold fresh airflows (Kalkstein and Corrigan,  
53 1986; Gimson, 1994; Hu et al., 2018; Ning et al., 2018b) or exacerbate air pollution by transporting air pollutants (Fu et al.,  
54 2008; Ding et al., 2013; Luo et al., 2018; Kang et al., 2019). Nevertheless, most of these studies did not consider the  
55 influences of diurnal cycles of cooling processes on air quality. Are the influences of cooling processes occurring during  
56 daytime and nighttime on air quality similar or different? There are two key questions. The first one is what are the behaviors  
57 of the diurnal cycles of atmospheric dispersion conditions and the second one is how these behaviors affect air quality,  
58 especially how the diurnal cycles of day-to-day temperature change affect air pollution. Exploring the answers to these  
59 questions is critical for fully understanding winter air pollution and is also urgently needed for improving air quality  
60 forecasting in China.

61  
62 Sichuan Basin (SCB) is one of the heaviest air pollution areas in China (Zhang et al., 2012; Ning et al., 2018a). With a high  
63 population density in SCB, its heavy air pollution thus poses serious health hazards to residents (Liao et al., 2017; Qiu et al.,  
64 2018; Zhu et al., 2018; Zhao et al., 2018). It is noted that SCB has a unique topography, with Qinling-Daba and Wu  
65 mountains in the north and east and with Qinghai-Tibet Plateau and Yunnan-Guizhou Plateau in the west and south of the  
66 basin (**Fig. 1**). The combination of these complex topography results in unique weather and climate, like the southwest

67 vortex and the Huaxi Autumn rain season etc. The southwest vortex, southern branch, and Qinghai-Tibet high pressure are  
68 often formed over SCB or Tibetan plateau and the complex synoptic systems significantly affect atmospheric dispersion  
69 conditions (Wang et al., 1993; Wei et al., 2014; Feng et al., 2016; Yu et al., 2016; Ning et al., 2019; Ning et al., 2020).  
70 Therefore, both the physical mechanism of atmospheric conditions' effects on air pollution and the air quality forecasting in  
71 SCB are more complicated than these in the eastern plain regions of China (Chen and Xie, 2012; Wang et al., 2014; Ning et  
72 al., 2019; Zhang et al., 2019). To better understand the formation mechanism of air pollution and improve air quality  
73 forecasting in mountain-basin areas, the effects of diurnal variations of atmospheric dispersion conditions on winter air  
74 quality in SCB call for urgent examinations.

75

76 The scientific goals of this study are to first cluster the typical diurnal cycles of day-to-day temperature change in SCB  
77 during wintertime and then to examine the mechanisms underlying the effects of the identified typical diurnal cycles on the  
78 following day-to-day air quality changes. We expect our study to better understand the physical mechanism of air quality  
79 evolutions and improve air pollution forecasting in mountain-basin areas. The rest of this paper is organized as below. Data  
80 and methodology are introduced in section 2. Section 3 describes the results of our study. Discussion related to our findings  
81 is given in section 4. Our conclusions are summarized in section 5.

## 82 **2. Data and methodology**

### 83 **2.1 Air quality data**

84 Hourly concentrations of surface  $PM_{2.5}$  (particulate matter with an aerodynamic diameter equal to or less than  $2.5 \mu m$ ),  $PM_{10}$   
85 (particulate matter with an aerodynamic diameter equal to or less than  $10 \mu m$ ),  $SO_2$  (sulfur dioxide),  $NO_2$  (nitrogen dioxide),  
86 and CO (carbon monoxide) in the winters (December–February) from December, 2014 to February, 2020 in 18 cities of SCB  
87 (**Fig. 1**) are obtained from the Ministry of Ecology and Environment of the People's Republic of China  
88 (<http://www.mee.gov.cn/xxgk2018/>). We calculate the city-wide average concentrations of the five air pollutants by  
89 arithmetically averaging their concentration at the national air quality monitoring sites located in the urban areas of that city,  
90 based on the technical regulation for ambient air quality assessment (on trial) (MEP, 2013; Ning et al., 2020). Among the 18  
91 cities in SCB, ten (Leshan, Meishan, Ziyang, Guangyuan, Bazhong, Ya'an, Dazhou, Suining, Guangan, and Neijiang) began  
92 monitoring air quality on January 1, 2015. Hence, the starting date of air quality data for these 10 cities is December 1, 2015.  
93 The starting date of air quality data for the rest 8 cities (Chengdu, Deyang, Mianyang, Zigong, Yibin, Luzhou, Nanchong and  
94 Chongqing) is December 1, 2014.

### 95 **2.2 Meteorological observational data**

96 Hourly winter surface temperature data observed at 105 meteorological stations in SCB (**Fig. 1**) from December 2006 to  
97 February 2020 are also collected. Their regional averages are used to determine the diurnal cycles of day-to-day temperature

98 change. Additionally, daily mean surface wind speed in the 18 cities of SCB is also collected. To explore the thermodynamic  
99 structure of the lower troposphere, daily potential temperature profiles at 20:00 Beijing time (BJT, UTC+8 h) from four  
100 sounding stations in SCB are also obtained. Four sounding stations, including Chengdu, Yibin, Dazhou, and Chongqing, are  
101 located in the northwest, southwest, northeast and southeast of the basin, respectively (See the orange dots in **Fig.1**). All  
102 these surface meteorological observations are obtained from the China Meteorological Administration (CMA)  
103 (<http://data.cma.cn/data/>).

### 104 **2.3 ERA-5 reanalysis data**

105 To obtain winter lower troposphere stability and reveal the possible mechanism of the formation of diurnal cycles of day-to-  
106 day temperature change, 700 hPa temperature, air pressure and air temperature at 2 m above the ground, total cloud cover,  $u$ -  
107 component wind and vertical velocity ( $w$ ) on multiple-pressure levels from December 2014 to February 2020 are collected  
108 from daily ERA-5 reanalysis data ( $0.25^\circ \times 0.25^\circ$  grids) (<https://cds.climate.copernicus.eu/cdsapp#!/dataset>). We collect the  
109 reanalysis data at four times each day (UTC 00:00, 06:00, 12:00 and 18:00) to calculate their daily mean values. The PBL  
110 height (PBLH) data at UTC 06:00 (14:00 BJT) are also obtained. PBLH is defined as the lowest model level where the bulk  
111 Richardson number first reaches the threshold value of 0.25 (Beljaars, 2006).

## 112 **2.4 Quantitative measurements of meteorological and air quality variables**

### 113 **2.4.1 Lower troposphere stability**

114 The lower troposphere stability (LTS) is defined as the differences in potential temperature between 700 hPa and the surface  
115 (Slingo, 1987). LTS can describe the thermal state of the lower troposphere and thus can evaluate the vertical mixing of air  
116 pollutants in the lower troposphere (Guo et al., 2016a; Guo et al., 2016b). A larger LTS indicates a stronger stability in the  
117 lower troposphere and a weaker vertical mixing of air pollutants.

### 118 **2.4.2 Day-to-day changes in meteorological conditions and air quality**

119 The day-to-day temperature change for each hour of a given day is defined by the hourly temperature differences between  
120 two neighboring days (Karl et al., 1995):

$$121 \quad \Delta T = T_i - T_{i-1} \quad (1)$$

122 where  $\Delta T$  refers to day-to-day temperature change,  $T_i$  and  $T_{i-1}$  are the hourly temperatures at the specific time of the day and  
123 the previous day, respectively. To reveal the possible mechanism of the formation of diurnal cycles of day-to-day  
124 temperature change, we calculate the day-to-day changes in total cloud cover at 06:00 BJT and 14:00 BJT, and also calculate  
125 the vertical west–east cross-sections of the day-to-day changes in wind vectors (synthesized by  $u$  and  $w$ ) at 14:00 BJT.

126

127 To investigate the effects of diurnal cycles of day-to-day temperature change on air quality, we also calculate the day-to-day  
128 changes in air pollutants concentrations and atmospheric dispersion conditions following the temperature change within one  
129 day. The following day-to-day changes in air pollutants concentrations (or atmospheric dispersion conditions) are defined by  
130 the differences in air pollutants concentrations (or meteorological conditions) between the next day and the current day:

$$131 \Delta PC = PC_{i+1} - PC_i \quad (2)$$

132 where  $PC$  represents PBLH, LTS, vertical potential temperature profiles (PT), surface wind speed (WS), or the  
133 concentrations of  $PM_{2.5}$ ,  $PM_{10}$ ,  $SO_2$ ,  $NO_2$ , and CO.  $\Delta PC$  represents the following day-to-day changes in PBLH, LTS, PT,  
134 WS, and five air pollutants concentrations.  $PC_{i+1}$  is the daily mean LTS, WS, and air pollutants concentrations, or the PBLH  
135 at 14:00 BJT and PT at 20:00 BJT on the next day.  $PC_i$  is the daily mean LTS, WS, and air pollutants concentrations, or the  
136 PBLH at 14:00 BJT and PT at 20:00 BJT on the current day.

## 137 2.5 K-means clustering

138 Clustering methods divide the objects into specific groups, with the goal that all data objects assigned to the same cluster  
139 have common characteristics while different clusters have distinct characteristics (Darby, 2005). The clustering methods  
140 have been widely used in climate and environmental researches (Bardossy et al., 1995; Cavazos, 2000; Luo and Lau, 2017;  
141 Bernier et al., 2019). In this study, the regional average values of day-to-day temperature change in SCB and the K-means  
142 clustering method (MacQueen, 1967) are selected to classify the diurnal cycles of day-to-day temperature change, because of  
143 the simplicity and convergence characteristics of K-means clustering method. The details of K-means clustering method can  
144 refer to MacQueen (1967) and (Mokdad and Haddad, 2017) and is also provided in the **supplementary document**.  
145 Additionally, the Calinski-Harabasz criterion, also known as the variance ratio criterion, is utilized to determine the optimal  
146 number of clusters (Caliński and Harabasz, 1974). The ultimate goal of Calinski-Harabasz criterion is to maximize the  
147 variance measure ratio of homogeneity within a cluster and heterogeneity between clusters (Chikumbo and Granville, 2019).

## 148 3. Results

### 149 3.1 Diurnal cycles of day-to-day temperature change

150 The selection of optimal number of clusters is illustrated in **Fig. 2**, which shows Calinski-Harabasz values associated with  
151 the numbers of clusters ranging from two to ten. The Calinski-Harabasz value with three clusters reaches the highest value,  
152 indicating that the optimal number of clustering is three. Three dominant diurnal cycles of day-to-day temperature change  
153 are therefore identified in SCB. The three typical diurnal cycles of day-to-day temperature change are depicted in **Fig. 3**. The  
154 days for *Cluster 1*, *Cluster 2*, and *Cluster 3* are 455 (accounting for 36.9 % of total days), 413 (33.5%), and 365 days  
155 (29.6%), respectively, indicating that the differences in the occurrence frequency among the three diurnal cycles are not

156 noticeable. However, the diurnal cycles of day-to-day temperature change among the three clusters exhibit obvious  
157 differences.

158

159 In particular, *Cluster 1* (diurnal cycle with increasing temperature), all the temperature changes are positive for 24 hours  
160 throughout all day, indicating that temperature increases during the past 24-hour and exhibits a maximum change  
161 approaching 1.5 °C between 16:00 BJT and 17:00 BJT. *Cluster 2* (diurnal cycle with decreasing temperature in the  
162 afternoon), the temperature changes show negative values after 12:00 BJT and drop to trough between 16:00 BJT and 17:00  
163 BJT with the minimum value of -1.5 °C, indicating that the cooling process is obvious in the afternoon. After 17:00 BJT, the  
164 absolute values of temperature change begin to decrease. The most prominent feature of *Cluster 2* is that the obvious  
165 decrease in temperature appears in the afternoon. *Cluster 3* (diurnal cycle with decreasing temperature in the morning), all  
166 temperature changes are negative for 24 hours throughout all day, and the obviously cooling process appears from 00:00 BJT  
167 to 09:00 BJT. The temperature changes show the minimum value approaching -1.5 °C between 07:00 BJT and 09:00 BJT.  
168 After 09:00 BJT, the absolute values of temperature change gradually reduce and are nearly close to zero in the afternoon.  
169 The most prominent feature of *Cluster 3* is that the obvious decrease in temperature appears in the morning.

170

171 To reveal the underlying mechanism of the formation of the above three diurnal cycles of day-to-day temperature change, we  
172 also investigate the nighttime and daytime day-to-day changes in total cloud cover that could play a key role in temperature  
173 changes by modulating atmospheric radiations. **Fig 4** shows the nighttime and daytime day-to-day changes in total cloud  
174 cover associated with the three diurnal cycles. Corresponding to the diurnal cycle with increasing temperature (*Cluster 1*),  
175 the total cloud exhibits slightly increase in the eastern of SCB, while decrease in the western of SCB (**Fig 4a**). The dipole  
176 spatial distribution could result in a weak changes in the regional average temperature across SCB during nighttime (**Fig 3**).  
177 During daytime, negative changes in total cloud cover are observed in the entire basin (**Fig 4d**) that are beneficial to the  
178 obviously increasing in temperature in the afternoon (**Fig 3**). On the contrary, both the nighttime and daytime changes in  
179 total cloud cover are positive in the entire basin for *Cluster 2* (**Fig 4b and e**), which could induce the increasing temperature  
180 during nighttime and decreasing temperature during afternoon (**Fig 3**). Corresponding to the diurnal cycle with decreasing  
181 temperature in the morning (*Cluster 3*), obviously decreasing in the total cloud cover are observed in the entire basin during  
182 nighttime (**Fig 4c**) that are beneficial to the temperature decreasing.

183

184 Moreover, SCB is located in the eastern Tibetan Plateau and the complex topography could play the key role in modulating  
185 the temperature changes over SCB (Ning et al., 2018b; Ning et al., 2019). Therefore, the vertical west–east cross-sections of  
186 the day-to-day changes in wind vectors (synthesized by  $u$  and  $w$ ) at 14:00 BJT are also investigated to uncover the physical  
187 and dynamics reasons of the formation of the above diurnal cycles of day-to-day temperature change. As shown in **Fig 5b**, a  
188 significantly ascending motion is observed over SCB that could induce the obviously decreasing temperature in the  
189 afternoon for *Cluster 2* (**Fig 3**). On the contrary, the descending motion prevails over SCB for *Cluster 1* and *Cluster 3*, which

190 is beneficial to the temperature increasing in the afternoon and thus plays a key role in the day-to-day temperature change for  
191 these two diurnal cycles.

### 192 3.2 Air quality in relation to the identified diurnal cycles

193 Heavy air pollution during winter in SCB is mainly caused by high concentrations of particulate matter (PM<sub>2.5</sub> and PM<sub>10</sub>)  
194 (Ning et al., 2018a). Therefore, the day-to-day changes in PM<sub>2.5</sub> and PM<sub>10</sub> concentrations following the three identified  
195 diurnal cycles within one day and the percentage values of the changes to the PM<sub>2.5</sub> and PM<sub>10</sub> concentrations in current day  
196 are investigated and are shown in **Fig. 6** and **Fig. S1**. **Fig. 6** depicts the spatial distributions of the following day-to-day  
197 changes in PM<sub>2.5</sub> and PM<sub>10</sub> concentrations associated with the three typical diurnal cycles. Under the diurnal cycle with  
198 increasing temperature (*Cluster 1*), nearly all parts of SCB experience increases in PM<sub>2.5</sub> and PM<sub>10</sub> concentrations on the  
199 following day (**Fig. 6a** and **d**) and the increases are up to about 10% of the PM<sub>2.5</sub> and PM<sub>10</sub> concentrations on the current day  
200 (**Fig. S1a** and **d**). The regional average changes in PM<sub>2.5</sub> and PM<sub>10</sub> concentrations are up to +3.95 µg/m<sup>3</sup> and +5.89 µg/m<sup>3</sup>,  
201 respectively.

202

203 On the contrary, negative changes in PM<sub>2.5</sub> and PM<sub>10</sub> concentrations are observed in the entire basin for the diurnal cycle  
204 with decreasing temperature in the afternoon (*Cluster 2*) (**Fig. 6b** and **e**) and account about 8% of the current day  
205 concentrations (**Fig. S1b** and **e**), indicating the improvement of air quality on the following day. The regional average  
206 changes in PM<sub>2.5</sub> and PM<sub>10</sub> concentrations are up to -8.93 µg/m<sup>3</sup> and -11.50 µg/m<sup>3</sup>, respectively. Under the diurnal cycle with  
207 decreasing temperature in the morning (*Cluster 3*), all parts of SCB experience increases in PM<sub>2.5</sub> and PM<sub>10</sub> concentrations  
208 (**Fig. 6c** and **f**) and these increases account 15% of current day concentrations (**Fig. S1c** and **f**), indicating the deterioration of  
209 air quality on the following day. It is noted that opposite changes in PM<sub>2.5</sub> and PM<sub>10</sub> concentrations are observed between  
210 *Cluster 3* and *Cluster 2* even though both of the two diurnal cycles show decreasing temperature. Compared with the diurnal  
211 cycle with increasing temperature (*Cluster 1*), the increases in PM<sub>2.5</sub> and PM<sub>10</sub> concentrations are larger for *Cluster 3*, and  
212 the regional average changes in PM<sub>2.5</sub> and PM<sub>10</sub> concentrations are up to +5.36 µg/m<sup>3</sup> and +5.91 µg/m<sup>3</sup>, respectively.

213

214 The contributions of gaseous pollutants in SCB to winter air pollution are also very important as SCB has a large number of  
215 motor vehicles and industries (Ning et al., 2018a). Therefore, the following day-to-day changes in three major gaseous (SO<sub>2</sub>,  
216 NO<sub>2</sub>, and CO) concentrations associated with the three diurnal cycles are also investigated. Similar to particulate matter, the  
217 relationships between the following day-to-day changes in gaseous pollutants concentrations and the three diurnal cycles are  
218 consistent with the results about PM<sub>2.5</sub> and PM<sub>10</sub>. As shown in **Fig. 6 g-o** and **Fig. S1 g-o**, nearly all parts of SCB experience  
219 increases in SO<sub>2</sub>, NO<sub>2</sub>, and CO concentrations on the following day for *Cluster 1* (diurnal cycle with increasing temperature)  
220 and *Cluster 3* (diurnal cycle with decreasing temperature in the morning). On the contrary, negative changes in SO<sub>2</sub>, NO<sub>2</sub>,  
221 and CO concentrations are observed in the entire basin for *Cluster 2* (diurnal cycle with decreasing temperature in the  
222 afternoon).

223

224 **Figs. 6** and **S1** collectively indicate that the air quality in SCB corresponding to *Cluster 1* and *Cluster 3* will deteriorate on  
225 the following day, while the air quality corresponding to *Cluster 2* will improve. These results suggest that the modulations  
226 of diurnal cycles of day-to-day temperature change on the following day-to-day changes in winter air quality are obvious and  
227 important. Thus, the diurnal cycles of day-to-day temperature change exhibit promising potential for winter air quality  
228 forecasting on the following day in SCB.

### 229 **3.3 Mechanism of the identified diurnal cycles effects on air quality**

230 To reveal the potential influence mechanism of the diurnal cycles of day-to-day temperature change on the following day-to-  
231 day changes in air quality, the atmospheric dispersion conditions corresponding to the three identified diurnal cycles are  
232 investigated. Firstly, the following day-to-day changes in PT vertical profiles at four sounding stations in SCB (**Fig. 7**) are  
233 examined to explore the thermodynamic structure in the lower troposphere. Then, the following day-to-day changes of the  
234 three meteorological parameters related to atmospheric dispersion conditions, including LTS (**Fig. 8a–c**), PBLH (**Fig. 8d–f**),  
235 and WS (**Fig. 8g–i**) are also investigated to evaluate the evolutions of atmospheric dispersion capacity.

236

237 Under the diurnal cycle with increasing temperature (*Cluster 1*), three sounding stations (Yibin, Dazhou, and Chongqing)  
238 experience increases in PT between 950 hPa to 800 hPa on the following day (**Fig. 7d, g, and j**). In Chengdu, decreased PT  
239 is observed below 900 hPa, while increased PT appears between 900 hPa to 750 hPa (**Fig. 7a**). All the PT profiles over the  
240 four sounding stations show higher temperature change in the higher level (800-850 hPa) than the lower level (900-950 hPa),  
241 which could enhance the atmospheric stability in the lower troposphere. As shown in **Fig.8a**, increased LTS are observed in  
242 most of the cities in SCB, indicating the atmospheric stratification in the lower troposphere becomes more stable. The stable  
243 atmospheric stratification inhibits the vertical mixing of the atmosphere and suppresses the development of PBL (Karppinen  
244 et al., 2001; Bei et al., 2016). As shown in **Fig. 8d**, obviously decreased PBLH are observed in all 18 cities of SCB.

245

246 Additionally, we also analyzed the following day-to-day changes in surface wind speed as the wind speed can represent the  
247 horizontal dispersion capacity of air pollutants (Lu et al., 2012; Deng et al., 2014). No noticeable decreases in wind speed  
248 appear in SCB (**Fig. 8g**). These results suggest that the diurnal cycle with increasing temperature (*Cluster 1*) enhances  
249 atmospheric stability in the lower troposphere, which can weaken the vertical exchange of airflow and then suppress the  
250 development of PBL, resulting in a small dispersion space of air pollutants and poor air quality in SCB on the following day.

251 Compared with *Cluster 1*, opposite vertical structure of PT changes (**Fig. 7b, e, h, and k**) is observed for the diurnal cycle  
252 with decreasing temperature in the afternoon (*Cluster 2*), which could weaken the atmospheric stability in the lower  
253 troposphere. As shown in **Fig. 8b**, negative changes in LTS appear in all parts of SCB, enhancing the vertical exchange of  
254 airflow and facilitating the development of PBL. As a result, increased PBLH is observed in all parts of SCB (**Fig. 8e**), and  
255 the regional average increment is up to 93.0 m. At the same time, the weakened atmospheric stability in the lower



256 troposphere is also conducive to the development of surface wind speed. As shown in **Fig. 8h**, the surface wind speed in the  
257 entire SCB is strengthened obviously, indicating the horizontal dispersion capacity of air pollutants is also improved. These  
258 results suggest that the diurnal cycle with decreasing temperature in the afternoon weakens atmospheric stability in the lower  
259 troposphere and creates good vertical mixing of airflow, which can promote the development of PBL and surface wind  
260 speed, facilitating the improvement of air quality on the following day.

261

262 For the Cluster 3, the PT changes are not noticeable below 850 hPa over the four sounding stations. As shown in **Fig. 7c, f, i**,  
263 and **1**, decreased PT is observed between 850 hPa and 700 hPa, while obviously increased PT appears above 700 hPa. This  
264 vertical structure of PT changes suggests that the atmospheric stability is enhanced above PBL over SCB, which is  
265 demonstrated playing a key role in the formation of winter heavy air pollution events in the basin (Ning et al., 2018b; Ning et  
266 al., 2019). As shown in **Fig. 8c**, increased LTS appears in the entire SCB, and the increments of LTS are obviously larger  
267 than those for *Cluster 1* (**Fig. 8a**), inhibiting the vertical mixing of atmosphere and suppressing the development of PBL. As  
268 a result, decreased PBLH is observed in all parts of SCB. Compared with *Cluster 1*, the enhanced atmospheric stability  
269 above PBL also suppresses the development of surface wind speed. As shown in **Fig. 8i**, all parts of SCB experience  
270 decreases in surface wind speed, weakening the horizontal dispersion capacity of air pollutants. These results suggest that  
271 both the vertical and horizontal dispersion capacity of air pollutants corresponding to *Cluster 3* are worse than those  
272 corresponding to *Cluster 1*. The differences in the atmospheric dispersion conditions between *Cluster 3* and *Cluster 1* can  
273 explain well that the air quality deterioration is more serious for *Cluster 3* than *Cluster 1* (**Fig. 6** and **Fig. S1**).

#### 274 **4. Discussion**

275 It's worth noting that the following day-to-day air quality changes between *Cluster 2* and *Cluster 3* in mountain-basin areas  
276 are opposite, even though both of the two diurnal cycles are associated with cooling processes. In the cases of the cooling  
277 process mainly occurring in the afternoon (*Cluster 2*), the atmospheric dispersion conditions are obviously improved,  
278 resulting in air quality improvement on the following day. On the contrary, the atmospheric dispersion conditions are  
279 obviously inhibited when the cooling process mainly appears in the morning (*Cluster 3*), resulting in air quality deterioration  
280 on the following day. These findings could improve our understanding of the effects of cooling processes on air quality  
281 (Kalkstein and Corrigan, 1986; Gimson, 1994; Hu et al., 2018; Ning et al., 2018b; Kang et al., 2019) and suggest that  
282 comprehensive investigations for the effects of diurnal cycles of atmospheric dispersion conditions on air quality are  
283 urgently needed in the future to fully understand the physical mechanism of air quality evolutions.

284

285 Additionally, both *Cluster 1* and *Cluster 3* are associated with weakened atmospheric dispersion conditions and lead to air  
286 quality deterioration on the following day. However, obvious differences in PT vertical profiles (**Fig. 7**) between *Cluster 1*  
287 and *Cluster 3* are observed. Especially for *Cluster 3*, decreased PT is observed between 850 hPa and 700 hPa, while

288 obviously increased PT appears above 700 hPa (**Fig. 7c, f, i, and l**). This special vertical structure of PT is closely related to  
289 the foehn that is formed under the synergistic effects of cooling processes and the Tibetan Plateau (Ning et al., 2019),  
290 indicating a stable layer exists above PBL and acts as a lid covering the PBL (Ning et al., 2018b; Ning et al., 2019). The  
291 vertical structure of PT are demonstrated playing key roles in the formation of winter heavy air pollution events in mountain-  
292 basin areas by inhibiting the development of secondary circulation and PBL (Ning et al., 2018b; Ning et al., 2019). These  
293 features suggest that the physical processes related to air pollution are more complex in mountain-basin areas than in the  
294 areas with flat terrain and urgently need to be further explored in the future.

295

296 Our study highlights that the following day-to-day air quality changes in mountain-basin areas are notably affected by the  
297 diurnal cycles of day-to-day temperature changes. We find that the identified diurnal cycles of day-to-day temperature  
298 variation in our study can explain well the evolutions of atmospheric dispersion conditions and air quality on the following  
299 day and thus could be useful for air quality forecasting in mountain-basin areas. Currently, numerical models (including  
300 WRF-Chem model and CMAQ model) (Grell et al., 2005; Byun and Ching, 1999) and statistical models (including statistical  
301 analysis, machine learning, and the hybrid linear–nonlinear method, etc.) (Huang, 1992; Chelani and Devotta, 2006; Borse,  
302 2020) are the two typical methods that have been widely used to forecast air quality by combining weather conditions and  
303 emission sources (Gidhagen et al., 2005). In the future, our findings should therefore be combined with numerical models or  
304 statistical models to improve air quality forecasting in mountain-basin areas.

## 305 **5. Conclusions**

306 Taking SCB as an example, this study is the first examination of the behaviors of diurnal cycles of day-to-day temperature  
307 change using hourly temperature observations and their effects on the following day-to-day air quality changes in mountain-  
308 basin areas. Three diurnal cycles of day-to-day temperature change are identified, which notably affect the following day-to-  
309 day air quality changes. Among them, two diurnal cycles (i.e., *Clusters 1 & 3*) inhibit atmospheric dispersion conditions by  
310 enhancing atmospheric stability, suppressing PBL, and weakening surface wind speed, thus leading to air quality  
311 deterioration on the following day.

312

313 Compared with the diurnal cycle with increasing temperature (i.e., *Cluster 1*), the atmospheric dispersion conditions are  
314 worse for the diurnal cycle with decreasing temperature in the morning (i.e., *Cluster 3*) and cause more serious deterioration  
315 of air quality. On the contrary, atmospheric dispersion condition with weakened atmospheric stability, deepened PBL, and  
316 enhanced surface wind speed is obviously improved for this type of diurnal cycle with decreasing temperature in the  
317 afternoon (i.e., *Cluster 2*), which improves the air quality on the following day. These results suggest that the identified  
318 diurnal cycles can explain well the evolutions of atmospheric dispersion conditions and air quality on the following day. Our  
319 findings exhibit promising potential for air quality forecasting in mountain-basin areas.

## 320 **Data availability**

321 The hourly air quality data were collected from the Ministry of Ecology and Environment of the People's Republic of China  
322 (<http://www.mee.gov.cn/xxgk2018/>). The meteorological observation data and the ERA-5 reanalysis data were obtained  
323 from the China Meteorological Administration (CMA) (<http://data.cma.cn/data/>) and the European Centre for Medium-  
324 Range Weather Forecasts (<https://cds.climate.copernicus.eu/cdsapp#!/dataset>), respectively.

## 325 **Author contributions**

326 DK performed data analysis, prepared the figures, and wrote original draft with contributions from all co-authors. GN  
327 designed the research and wrote the manuscript. SW, ML, XN, and MM provided interpretation and editing of the  
328 manuscript. JC performed data analysis and provided useful comments.

## 329 **Competing interests**

330 The authors declare that they have no conflict of interest.

## 331 **Acknowledgements**

332 This work was supported by the National Natural Science Foundation of China (91644226, 41871029, 41830648, and  
333 41771453), the Major Scientific and Technological Projects in Sichuan Province (2018SZDZX0023), the Applied Basic  
334 Research Project of Sichuan Science and Technology Department (2020YJ0425), the Technology Innovation Research and  
335 Development Project of Chengdu Science and Technology Department (2018-YF05-00219-SN), the National Major Projects  
336 on High-Resolution Earth Observation System (21-Y20B01-9001-19/22), and the appointment of M. Luo at Sun Yat-sen  
337 University is partially supported by the Pearl River Talent Recruitment Program of Guangdong Province, China  
338 (2017GC010634). We would like to thank the following departments for the provided data, the Ministry of Ecology and  
339 Environment of the People's Republic of China, the China Meteorological Administration, and the European Centre for  
340 Medium-Range Weather Forecasts. The authors are thankful to the anonymous reviewers who provided valuable comments  
341 and suggestions.

## 342 **References**

343 Bardossy, A., Duckstein, L., and Bogardi, I.: Fuzzy rule-based classification of atmospheric circulation patterns, *Int. J.*  
344 *Climatol.*, 15, 1087-1097, doi: 10.1002/joc.3370151003, 1995.

345 Bei, N., Xiao, B., Meng, N., and Feng, T.: Critical role of meteorological conditions in a persistent haze episode in the  
346 Guanzhong basin, China, *Sci. Total Environ.*, 550, 273-284, doi: 10.1016/j.scitotenv.2015.12.159, 2016.

347 Beljaars, A.: Chapter 3: Turbulent transport and interactions with the surface, Part IV: physical processes, IFS  
348 documentation, operational implementation 12 September 2006 Cy31r1 31, ECMWF, Shinfield Park, Reading, RG2 9AX,  
349 England, 2006.

350 Bernier, C., Wang, Y., Estes, M., Lei, R., Jia, B., Wang, S.-C., and Sun, J.: Clustering surface ozone diurnal cycles to  
351 understand the impact of circulation patterns in Houston, TX, *J. Geophys. Res. Atmos.*, 124, 13457-13474, doi:  
352 10.1029/2019JD031725, 2019.

353 Borse, S. K.: A Review: predicting air quality using different technique, *Acta technica corviniensis-bulletin of engineering*,  
354 13, 153-157, 2020.

355 Byun, D., and Ching, J.: Science algorithms of the EPA models-3 community multiscale air quality model (CMAQ)  
356 modeling system, Rep. EPA/600/R-99, U.S. Environmental Protection Agency, Research Triangle Park, NC, 1999.

357 Caliński, T., and Harabasz, J.: A dendrite method for cluster analysis, *Communications in Statistics*, 3, 1-27, doi:  
358 10.1080/03610927408827101, 1974.

359 Cavazos, T.: Using self-organizing maps to investigate extreme climate events: an application to wintertime precipitation in  
360 the Balkans, *J. Clim.*, 13, 1718-1732, doi: 10.1175/1520-0442(2000)013<1718:USOMTI>2.0.CO;2, 2000.

361 Chelani, A. B., and Devotta, S.: Air quality forecasting using a hybrid autoregressive and nonlinear model, *Atmos. Environ.*,  
362 40, 1774-1780, doi: 10.1016/j.atmosenv.2005.11.019, 2006.

363 Chen, Y., and Xie, S.: Temporal and spatial visibility trends in the Sichuan Basin, China, 1973 to 2010, *Atmos. Res.*, 112,  
364 25-34, doi: 10.1016/j.atmosres.2012.04.009, 2012.

365 Chikumbo, O., and Granville, V.: Optimal clustering and cluster identity in understanding high-dimensional data spaces with  
366 tightly distributed points, *Mach. Learn. Knowl. Extr.*, 1, 715-744, doi: 10.3390/make1020042, 2019.

367 Darby, L. S.: Cluster analysis of surface winds in Houston, Texas, and the impact of wind patterns on ozone, *J. Appl.*  
368 *Meteorol. Climatol.*, 44, 1788-1806, doi: 10.1175/JAM2320.1, 2005.

369 Deng, T., Wu, D., Deng, X., Tan, H., Li, F., and Liao, B.: A vertical sounding of severe haze process in Guangzhou area,  
370 *Sci. China Earth Sci.*, 57, 2650-2656, doi: 10.1007/s11430-014-4928-y, 2014.

371 Ding, A., Wang, T., and Fu, C.: Transport characteristics and origins of carbon monoxide and ozone in Hong Kong, South  
372 China, *J. Geophys. Res. Atmos.*, 118, 9475-9488, doi: 10.1002/jgrd.50714, 2013.

373 Dong, Y., Li, J., Guo, J., Jiang, Z., Chu, Y., Chang, L., Yang, Y., and Liao, H.: The impact of synoptic patterns on  
374 summertime ozone pollution in the North China Plain, *Sci. Total Environ.*, 735, 139559, doi:  
375 10.1016/j.scitotenv.2020.139559, 2020.

376 Feng, X., Liu, C., Fan, G., Liu, X., and Feng, C.: Climatology and structures of southwest vortices in the NCEP climate  
377 forecast system reanalysis, *J. Clim.*, 29, 7675-7701, doi: 10.1175/JCLI-D-15-0813.1, 2016.

378 Feng, X., Wei, S., and Wang, S.: Temperature inversions in the atmospheric boundary layer and lower troposphere over the  
379 Sichuan Basin, China: climatology and impacts on air pollution, *Sci. Total Environ.*, 726, 138579, doi:  
380 10.1016/j.scitotenv.2020.138579, 2020.

381 Fu, Q., Zhuang, G., Wang, J., Xu, C., Huang, K., Li, J., Hou, B., Lu, T., and Streets, D. G.: Mechanism of formation of the  
382 heaviest pollution episode ever recorded in the Yangtze River Delta, China, *Atmos. Environ.*, 42, 2023-2036, doi:  
383 10.1016/j.atmosenv.2007.12.002, 2008.

384 Gidhagen, L., Johansson, C., Langner, J., and Foltescu, V. L.: Urban scale modeling of particle number concentration in  
385 Stockholm, *Atmos. Environ.*, 39, 1711-1725, doi: 10.1016/j.atmosenv.2004.11.042, 2005.

386 Gimson, N. R.: Dispersion and removal of pollutants during the passage of an atmospheric frontal system, *Q. J. R. Meteorol.*  
387 *Soc.*, 120, 139-160, doi: 10.1002/qj.49712051509, 1994.

388 Grell, G. A., Peckham, S. E., Schmitz, R., McKeen, S. A., Frost, G., Skamarock, W. C., and Eder, B.: Fully coupled “online”  
389 chemistry within the WRF model, *Atmos. Environ.*, 39, 6957-6975, doi: 10.1016/j.atmosenv.2005.04.027, 2005.

390 Guo, J., Deng, M., Lee, S. S., Wang, F., Li, Z., Zhai, P., Liu, H., Lv, W., Yao, W., and Li, X.: Delaying precipitation and  
391 lightning by air pollution over the Pearl River Delta. Part I: observational analyses, *J. Geophys. Res. Atmos.*, 121, 6472-  
392 6488, doi: 10.1002/2015JD023257, 2016a.

393 Guo, J., Miao, Y., Zhang, Y., Liu, H., Li, Z., Zhang, W., He, J., Lou, M., Yan, Y., Bian, L., and Zhai, P.: The climatology of  
394 planetary boundary layer height in China derived from radiosonde and reanalysis data, *Atmos. Chem. Phys.*, 16, 13309-  
395 13319, doi: 10.5194/acp-16-13309-2016, 2016b.

396 Guo, J., Chen, X., Su, T., Liu, L., Zheng, Y., Chen, D., Li, J., Xu, H., Lv, Y., and He, B.: The climatology of lower  
397 tropospheric temperature inversions in China from radiosonde measurements: roles of black carbon, local meteorology,  
398 and large-scale subsidence, *J. Clim.*, 33, 9327-9350, doi: 10.1175/JCLI-D-19-0278.1, 2020.

399 Hu, Y., Wang, S., Ning, G., Zhang, Y., Wang, J., and Shang, Z.: A quantitative assessment of the air pollution purification  
400 effect of a super strong cold-air outbreak in January 2016 in China, *Air Qual. Atmos. Hlth.*, 11, 907-923, doi:  
401 10.1007/s11869-018-0592-2, 2018.

402 Huang, G.: A stepwise cluster analysis method for predicting air quality in an urban environment, *Atmos. Environ. Part B.*  
403 *Urb. Atmos.*, 26, 349-357, doi: 10.1016/0957-1272(92)90010-P, 1992.

404 Kalkstein, L. S., and Corrigan, P.: A Synoptic climatological approach for geographical analysis: assessment of sulfur  
405 dioxide concentrations, *Ann. Assoc. Am. Geogr.*, 76, 381-395, doi: 10.1111/j.1467-8306.1986.tb00126.x, 1986.

406 Kang, H., Zhu, B., Gao, J., He, Y., Wang, H., Su, J., Pan, C., Zhu, T., and Yu, B.: Potential impacts of cold frontal passage  
407 on air quality over the Yangtze River Delta, China, *Atmos. Chem. Phys.*, 19, 3673-3685, doi: 10.5194/acp-19-3673-2019,  
408 2019.

409 Karl, T. R., Knight, R. W., and Plummer, N.: Trends in high-frequency climate variability in the twentieth century, *Nature*,  
410 377, 217-220, doi: 10.1038/377217a0, 1995.

411 Karppinen, A., Joffre, S. M., Kukkonen, J., and Bremer, P.: Evaluation of inversion strengths and mixing heights during  
412 extremely stable atmospheric stratification, *Int. J. Environ. Pollut.*, 16, 603-613, doi: 10.1504/IJEP.2001.000653, 2001.

413 Kelly, F. J., and Zhu, T.: Transport solutions for cleaner air, *Science*, 352, 934-936, doi: 10.1126/science.aaf3420, 2016.

414 Li, Y., Chen, Q., Zhao, H., Wang, L., and Tao, R.: Variations in PM<sub>10</sub>, PM<sub>2.5</sub> and PM<sub>1.0</sub> in an urban area of the Sichuan Basin  
415 and their relation to meteorological factors, *Atmosphere*, 6, 150-163, 2015.

416 Li, Z., Guo, J., Ding, A., Liao, H., Liu, J., Sun, Y., Wang, T., Xue, H., Zhang, H., and Zhu, B.: Aerosol and boundary-layer  
417 interactions and impact on air quality, *Natl. Sci. Rev.*, 4, 810-833, doi: 10.1093/nsr/nwx117, 2017.

418 Liao, T., Wang, S., Ai, J., Gui, K., Duan, B., Zhao, Q., Zhang, X., Jiang, W., and Sun, Y.: Heavy pollution episodes,  
419 transport pathways and potential sources of PM<sub>2.5</sub> during the winter of 2013 in Chengdu (China), *Sci. Total Environ.*, 584-  
420 585, 1056-1065, doi: 10.1016/j.scitotenv.2017.01.160, 2017.

421 Lu, C., Deng, Q.-h., Liu, W.-w., Huang, B.-l., and Shi, L.-z.: Characteristics of ventilation coefficient and its impact on  
422 urban air pollution, *J. Cent. South Univ.*, 19, 615-622, doi: 10.1007/s11771-012-1047-9, 2012.

423 Luo, M., and Lau, N.-C.: Heat waves in southern China: synoptic behavior, long-term change, and urbanization effects, *J.*  
424 *Clim.*, 30, 703-720, doi: 10.1175/JCLI-D-16-0269.1, 2017.

425 Luo, M., Hou, X., Gu, Y., Lau, N.-C., and Yim, S. H.-L.: Trans-boundary air pollution in a city under various atmospheric  
426 conditions, *Sci. Total Environ.*, 618, 132-141, doi: 10.1016/j.scitotenv.2017.11.001, 2018.

427 MacQueen, J.: Some methods for classification and analysis of multivariate observations, *Proceedings of the fifth Berkeley*  
428 *symposium on mathematical statistics and probability*, 1967, 281-297.

429 MEP: Technical regulation on ambient air quality assessment (on trial) (HJ663-2013), China Environmental Science Press,  
430 Beijing, China, 2013.

431 Miao, Y., Guo, J., Liu, S., Liu, H., Li, Z., Zhang, W., and Zhai, P.: Classification of summertime synoptic patterns in Beijing  
432 and their associations with boundary layer structure affecting aerosol pollution, *Atmos. Chem. Phys.*, 17, 3097-3110, doi:  
433 10.5194/acp-17-3097-2017, 2017.

434 Miao, Y., Liu, S., Guo, J., Huang, S., Yan, Y., and Lou, M.: Unraveling the relationships between boundary layer height and  
435 PM<sub>2.5</sub> pollution in China based on four-year radiosonde measurements, *Environ. Pollut.*, 243, 1186-1195, doi:  
436 10.1016/j.envpol.2018.09.070, 2018.

437 Mokdad, F., and Haddad, B.: Improved infrared precipitation estimation approaches based on k-means clustering:  
438 application to north Algeria using MSG-SEVIRI satellite data, *Adv. Space Res.*, 59, 2880-2900, doi:  
439 10.1016/j.asr.2017.03.027, 2017.

440 Ning, G., Wang, S., Ma, M., Ni, C., Shang, Z., Wang, J., and Li, J.: Characteristics of air pollution in different zones of  
441 Sichuan Basin, China, *Sci. Total Environ.*, 612, 975-984, doi: 10.1016/j.scitotenv.2017.08.205, 2018a.

442 Ning, G., Wang, S., Yim, S. H. L., Li, J., Hu, Y., Shang, Z., Wang, J., and Wang, J.: Impact of low-pressure systems on  
443 winter heavy air pollution in the northwest Sichuan Basin, China, *Atmos. Chem. Phys.*, 18, 13601-13615, doi:  
444 10.5194/acp-18-13601-2018, 2018b.

445 Ning, G., Yim, S. H. L., Wang, S., Duan, B., Nie, C., Yang, X., Wang, J., and Shang, K.: Synergistic effects of synoptic  
446 weather patterns and topography on air quality: a case of the Sichuan Basin of China, *Clim. Dyn.*, 53, 6729-6744,  
447 doi:10.1007/s00382-019-04954-3, 2019.

448 Ning, G., Yim, S. H. L., Yang, Y., Gu, Y., and Dong, G.: Modulations of synoptic and climatic changes on ozone pollution  
449 and its health risks in mountain-basin areas, *Atmos. Environ.*, 240, 117808, doi: 10.1016/j.atmosenv.2020.117808, 2020.

450 Qiu, H., Yu, H., Wang, L., Zhu, X., Chen, M., Zhou, L., Deng, R., Zhang, Y., Pu, X., and Pan, J.: The burden of overall and  
451 cause-specific respiratory morbidity due to ambient air pollution in Sichuan Basin, China: a multi-city time-series  
452 analysis, *Environ. Res.*, 167, 428-436, doi: 10.1016/j.envres.2018.08.011, 2018.

453 Slingo, J. M.: The development and verification of a cloud prediction scheme for the ECMWF model, *Q. J. Roy. Meteor.*  
454 *Soc.*, 113, 899-927, doi: 10.1002/qj.49711347710, 1987.

455 Streets, D. G., Gupta, S., Waldhoff, S. T., Wang, M. Q., Bond, T. C., and Yiyun, B.: Black carbon emissions in China,  
456 *Atmos. Environ.*, 35, 4281-4296, doi: 10.1016/S1352-2310(01)00179-0, 2001.

457 Su, T., Li, Z., Zheng, Y., Luan, Q., and Guo, J.: Abnormally shallow boundary layer associated with severe air pollution  
458 during the COVID-19 lockdown in China, *Geophys. Res. Lett.*, 47, e2020GL090041, doi: 10.1029/2020GL090041, 2020.

459 Wang, W., Kuo, Y.-H., and Warner, T. T.: A diabatically driven mesoscale vortex in the lee of the Tibetan Plateau, *Mon.*  
460 *Weather Rev.*, 121, 2542-2561, doi: 10.1175/1520-0493(1993)121<2542:ADDMVI>2.0.CO;2, 1993.

461 Wang, X., Dickinson, R. E., Su, L., Zhou, C., and Wang, K.: PM<sub>2.5</sub> pollution in China and how it has been exacerbated by  
462 terrain and meteorological conditions, *Bull. Am. Meteorol. Soc.*, 99, 105-119, doi: 10.1175/BAMS-D-16-0301.1, 2018.

463 Wang, Y., Yao, L., Wang, L., Liu, Z., Ji, D., Tang, G., Zhang, J., Sun, Y., Hu, B., and Xin, J.: Mechanism for the formation  
464 of the January 2013 heavy haze pollution episode over central and eastern China, *Sci. China Earth Sci.*, 57, 14-25, doi:  
465 10.1007/s11430-013-4773-4, 2014.

466 Wei, P., Cheng, S., Li, J., and Su, F.: Impact of boundary-layer anticyclonic weather system on regional air quality, *Atmos.*  
467 *Environ.*, 45, 2453-2463, doi: 10.1016/j.atmosenv.2011.01.045, 2011.

468 Wei, W., Zhang, R., Wen, M., Rong, X., and Li, T.: Impact of Indian summer monsoon on the South Asian High and its  
469 influence on summer rainfall over China, *Clim. Dyn.*, 43, 1257-1269, doi: 10.1007/s00382-013-1938-y, 2014.

470 Xiao, Q., Ma, Z., Li, S., and Liu, Y.: The impact of winter heating on air pollution in China, *PLoS One*, 10, e0117311, doi:  
471 10.1371/journal.pone.0117311, 2015.

472 Xu, T., Song, Y., Liu, M., Cai, X., Zhang, H., Guo, J., and Zhu, T.: Temperature inversions in severe polluted days derived  
473 from radiosonde data in North China from 2011 to 2016, *Sci. Total Environ.*, 647, 1011-1020, doi:  
474 10.1016/j.scitotenv.2018.08.088, 2019.

475 Yarnal, B.: *Synoptic climatology in environmental analysis: a primer*, Belhaven Press, London, 1993.

476 Ye, X., Song, Y., Cai, X., and Zhang, H.: Study on the synoptic flow patterns and boundary layer process of the severe haze  
477 events over the North China Plain in January 2013, *Atmos. Environ.*, 124, 129-145, doi: 10.1016/j.atmosenv.2015.06.011,  
478 2016.

479 Yu, S., Gao, W., Xiao, D., and Peng, J.: Observational facts regarding the joint activities of the southwest vortex and plateau  
480 vortex after its departure from the Tibetan Plateau, *Adv. Atmos. Sci.*, 33, 34-46, doi :10.1007/s00376-015-5039-1, 2016.

481 Zhang, L., Guo, X., Zhao, T., Gong, S., Xu, X., Li, Y., Luo, L., Gui, K., Wang, H., Zheng, Y., and Yin, X.: A modelling  
482 study of the terrain effects on haze pollution in the Sichuan Basin, *Atmos. Environ.*, 196, 77-85, doi:  
483 10.1016/j.atmosenv.2018.10.007, 2019.

484 Zhang, Q., Streets, D. G., Carmichael, G. R., He, K. B., Huo, H., Kannari, A., Klimont, Z., Park, I. S., Reddy, S., Fu, J. S.,  
485 Chen, D., Duan, L., Lei, Y., Wang, L. T., and Yao, Z. L.: Asian emissions in 2006 for the NASA INTEX-B mission,  
486 *Atmos. Chem. Phys.*, 9, 5131-5153, doi: 10.5194/acp-9-5131-2009, 2009.

487 Zhang, X. Y., Wang, Y. Q., Niu, T., Zhang, X. C., Gong, S. L., Zhang, Y. M., and Sun, J. Y.: Atmospheric aerosol  
488 compositions in China: spatial/temporal variability, chemical signature, regional haze distribution and comparisons with  
489 global aerosols, *Atmos. Chem. Phys.*, 12, 779-799, doi: 10.5194/acp-12-779-2012, 2012.

490 Zhang, Y., Guo, J., Yang, Y., Wang, Y., and Yim, S. H. L.: Vertical wind shear modulates particulate matter pollutions: A  
491 perspective from radar wind profiler observations in Beijing, China, *Remote Sens.*, 12, 546, 2020.

492 Zhang, Z., Zhang, X., Gong, D., Kim, S. J., Mao, R., and Zhao, X.: Possible influence of atmospheric circulations on winter  
493 haze pollution in the Beijing–Tianjin–Hebei region, northern China, *Atmos. Chem. Phys.*, 16, 561-571, doi: 10.5194/acp-  
494 16-561-2016, 2016.

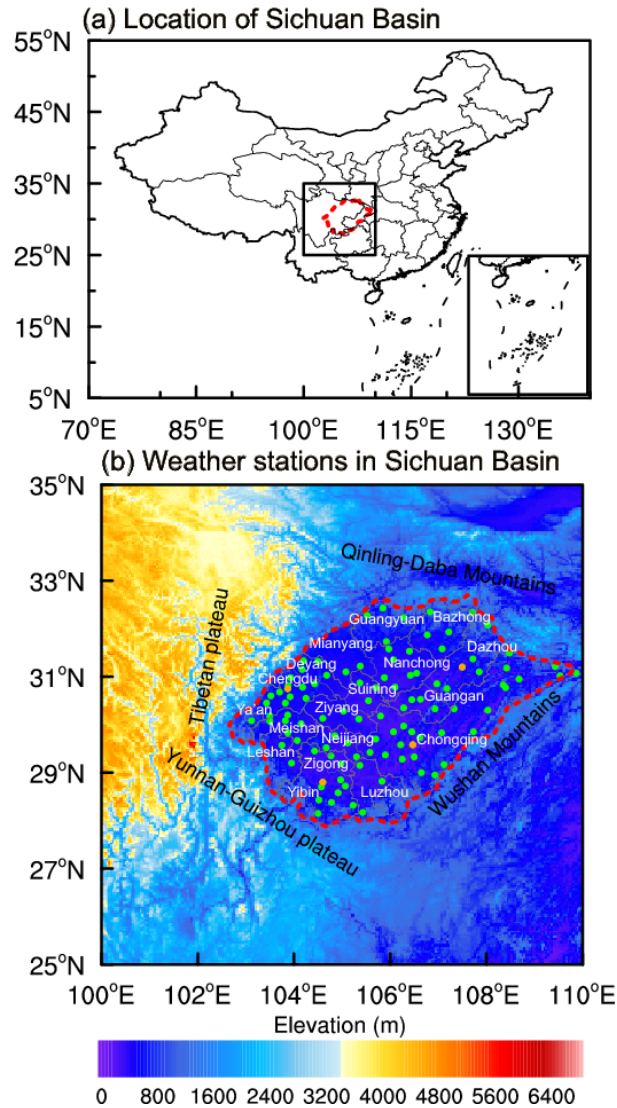
495 Zhao, S., Yu, Y., Yin, D., Qin, D., He, J., and Dong, L.: Spatial patterns and temporal variations of six criteria air pollutants  
496 during 2015 to 2017 in the city clusters of Sichuan Basin, China, *Sci. Total Environ.*, 624, 540-557, doi:  
497 10.1016/j.scitotenv.2017.12.172, 2018.

498 Zhu, S., Xia, L., Wu, J., Chen, S., Chen, F., Zeng, F., Chen, X., Chen, C., Xia, Y., Zhao, X., and Zhang, J.: Ambient air  
499 pollutants are associated with newly diagnosed tuberculosis: a time-series study in Chengdu, China, *Sci. Total Environ.*,  
500 631-632, 47-55, doi: 10.1016/j.scitotenv.2018.03.017, 2018.

501

502





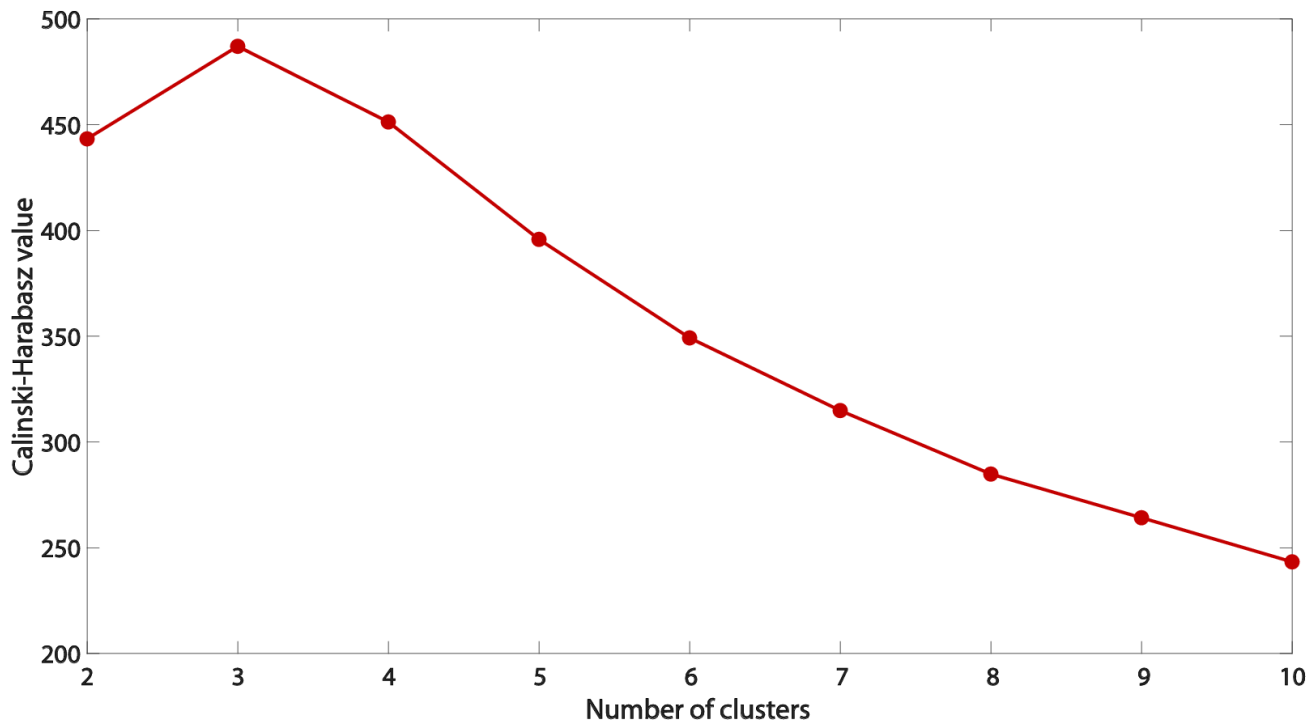
505

506 **Figure 1** Map of Sichuan Basin (SCB) in Southwest China. (a) Location of SCB; (b) Topography of SCB (shading) and the

507 spatial distribution of 105 meteorological stations (dots) in SCB. The dashed red line indicates the border of SCB. The

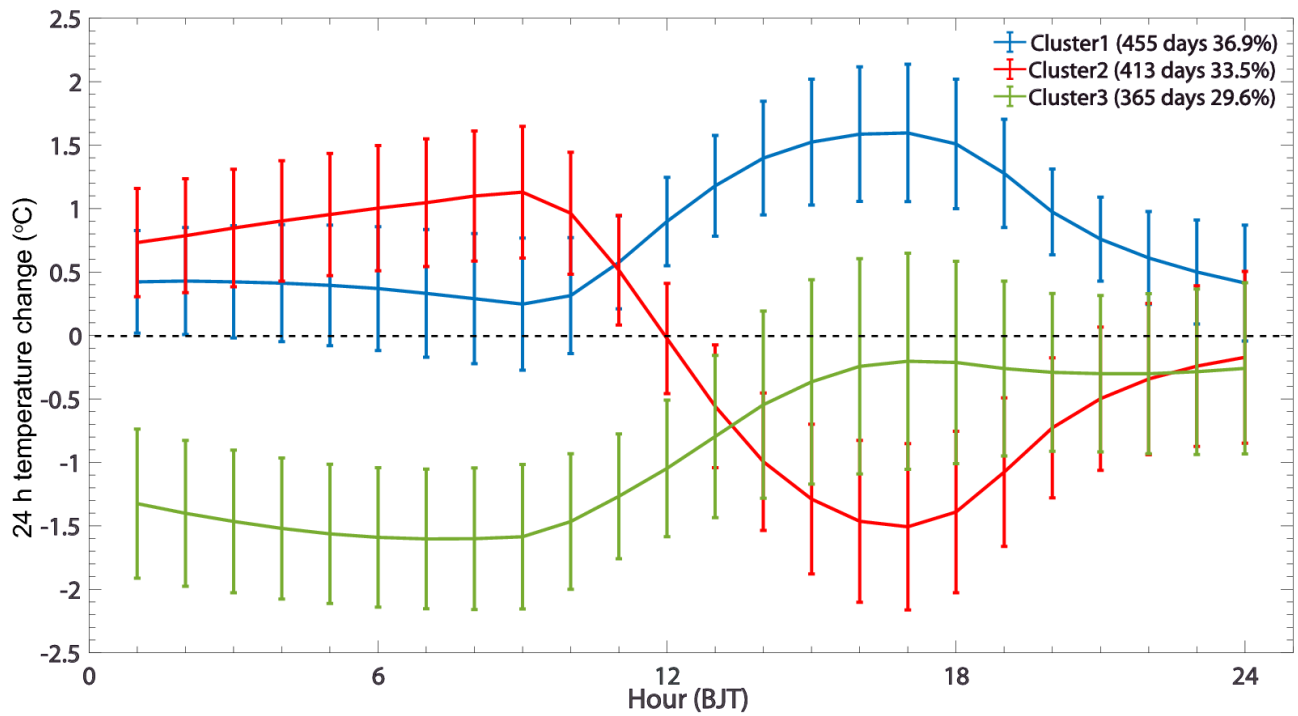
508 orange dots indicate the meteorological stations with radiosonde measurements. The white text indicate the name of the

509 major cities in SCB.



510

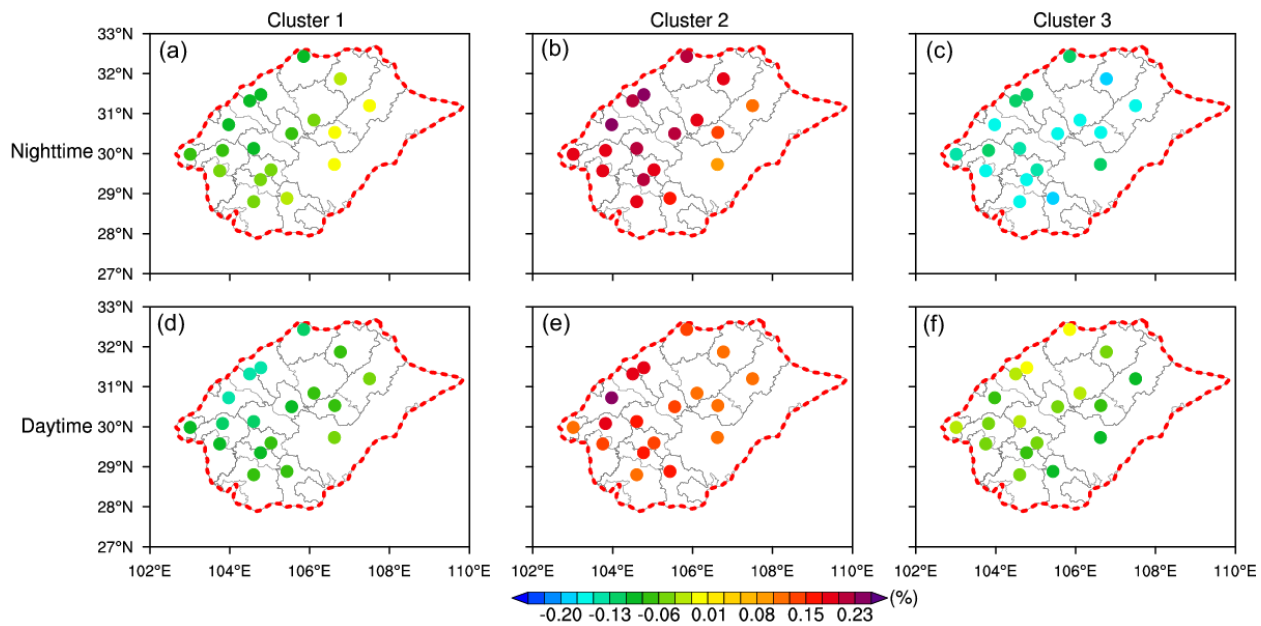
511 **Figure 2** Changes of Calinski-Harabasz values with different numbers of identified clusters.



513

514 **Figure 3** Three identified diurnal cycles of day-to-day temperature change based on the K-means clustering method. The  
 515 error bar denotes the standard deviation of day-to-day temperature change.

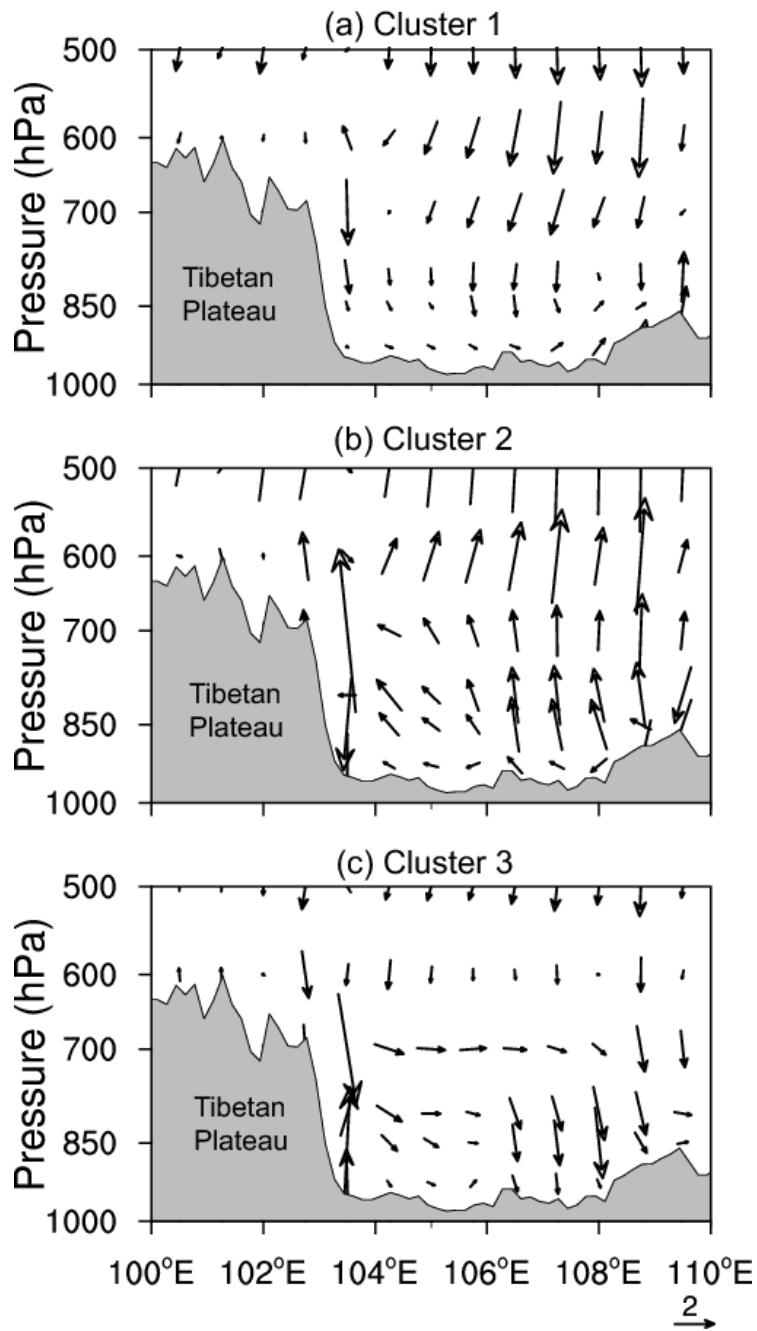
516



517

518 **Figure 4** The nighttime (a-c) and daytime (d-f) day-to-day changes in total cloud cover associated with the three diurnal  
 519 cycles.

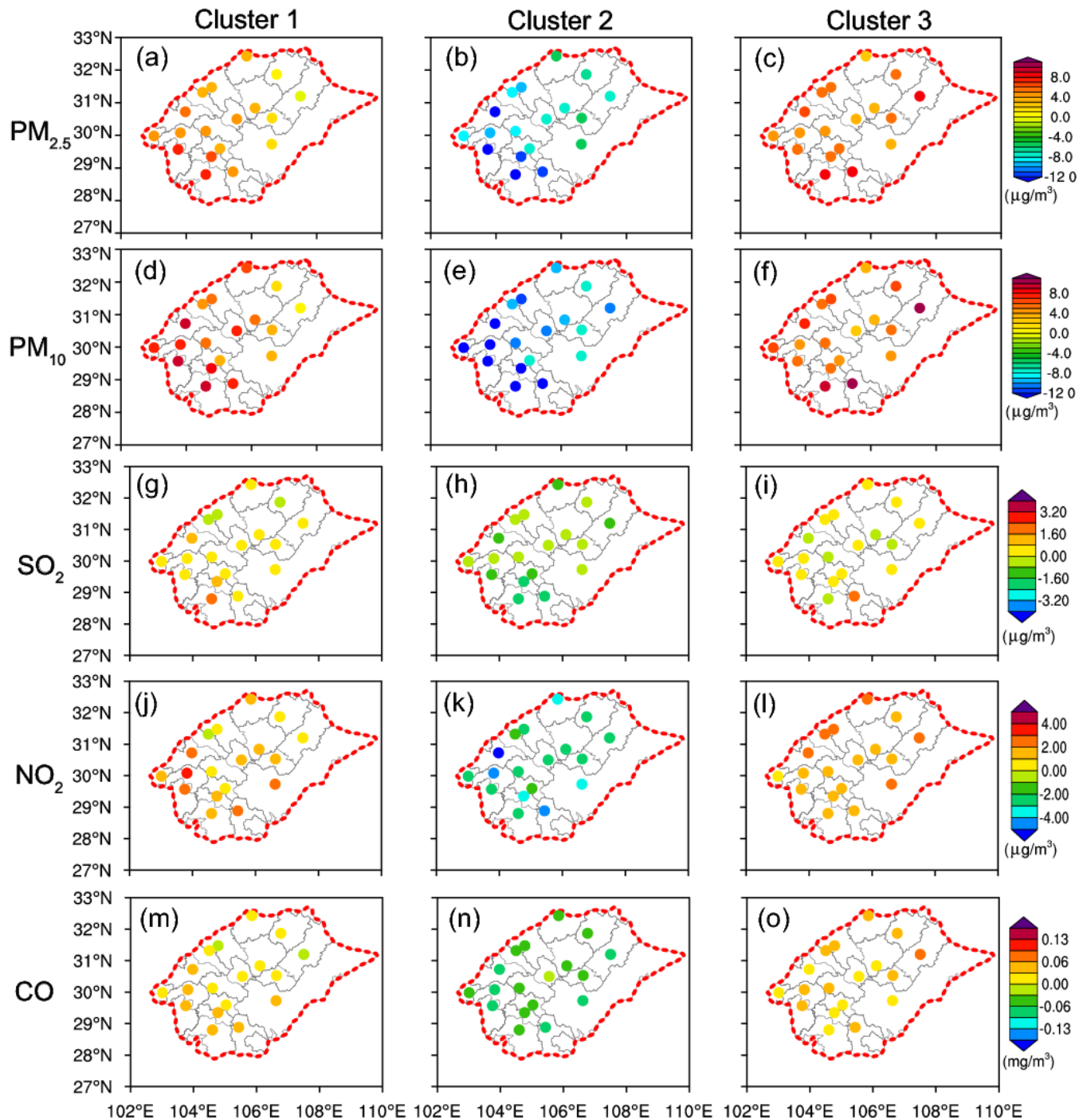
520



521

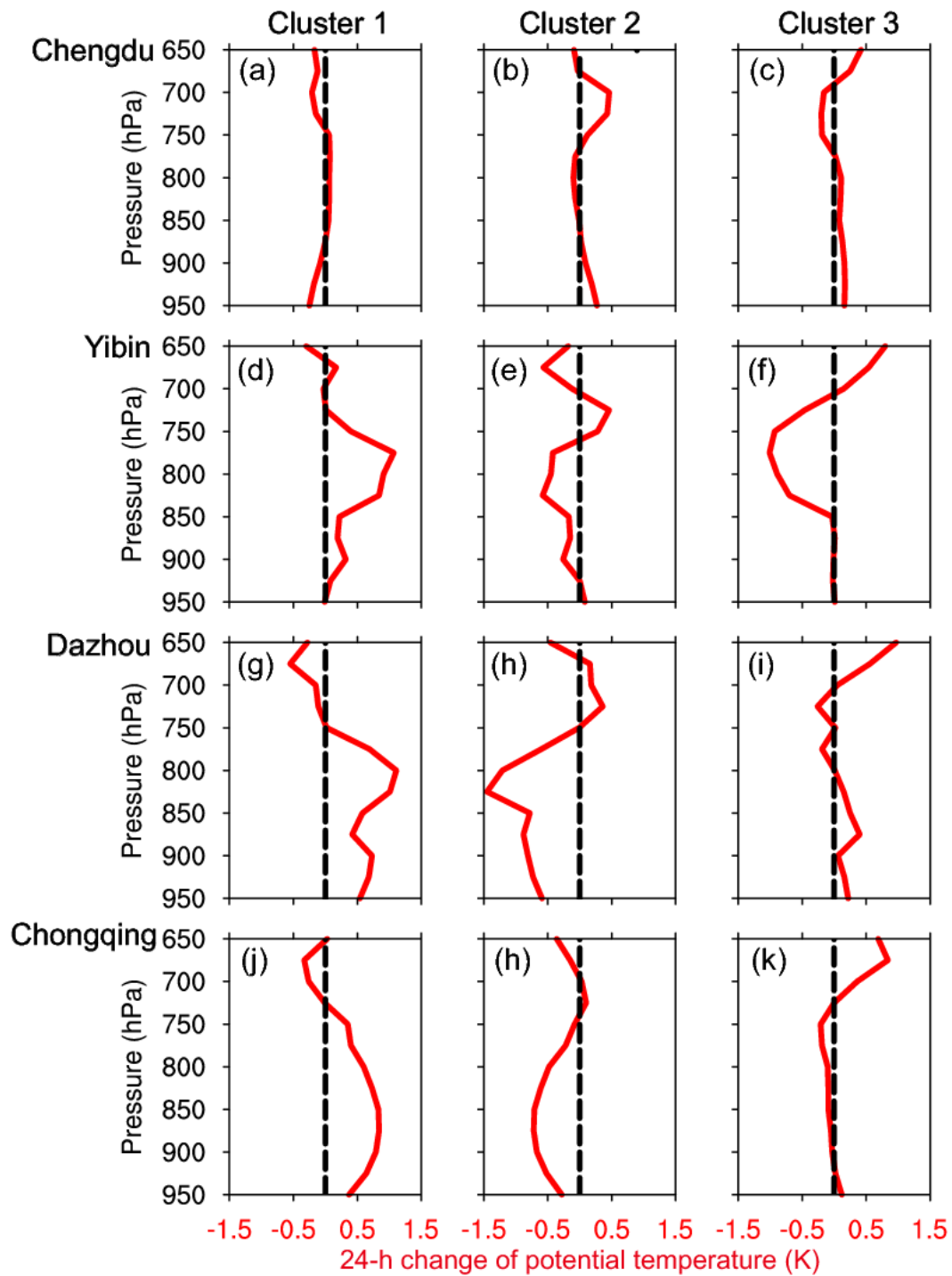
522 **Figure 5** Vertical west-east cross-sections of the day-to-day changes in wind vectors (synthesized by  $u$  and  $w$ ) at 14:00 BJT  
 523 through the SCB (30.75°N) associated with the three diurnal cycles. Note that the vertical velocity is multiplied by -50 when  
 524 plotting the wind vectors. The units for  $u$  and  $w$  are m/s and Pa/s, respectively. The complex terrain is marked by grey  
 525 shading.

526



528

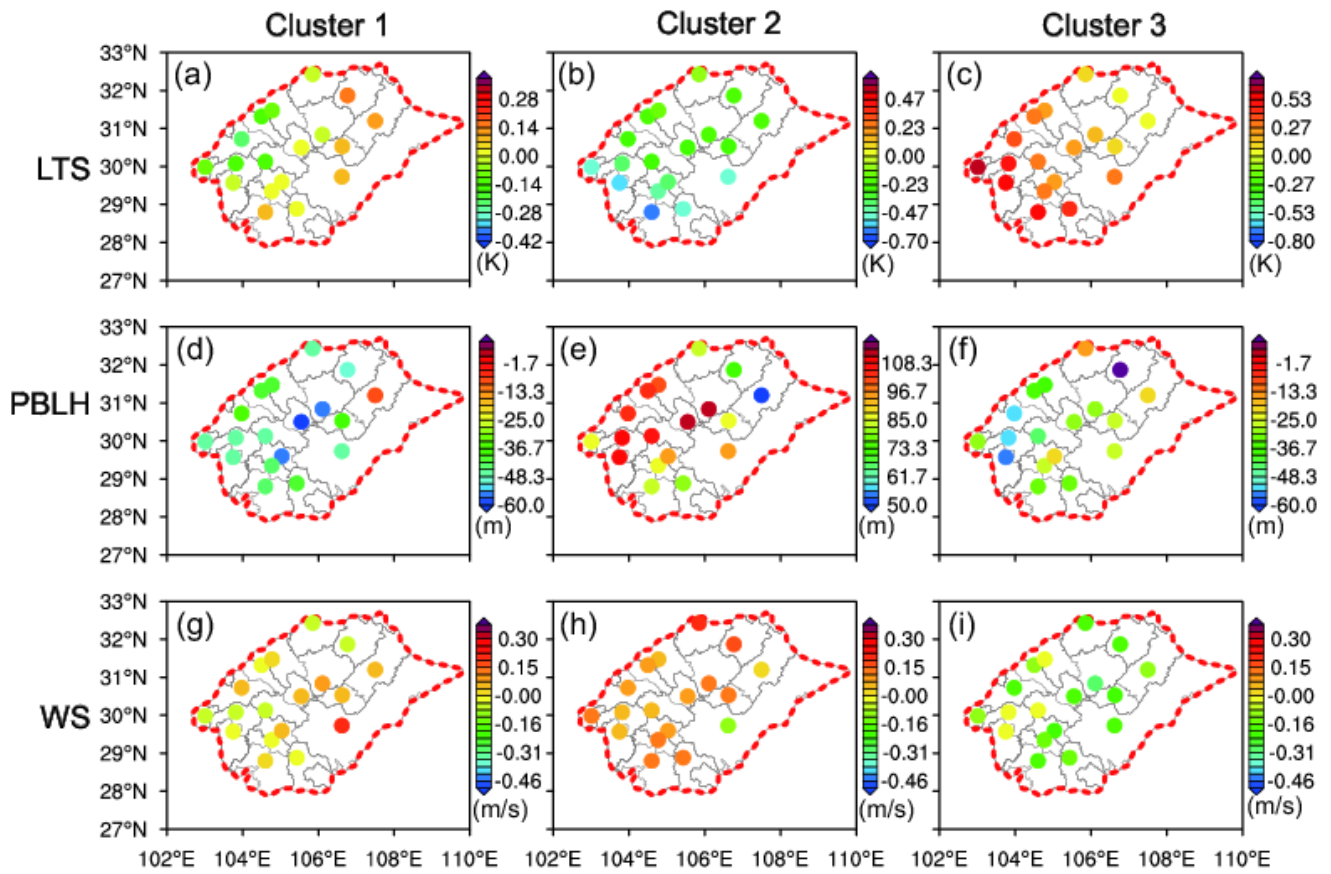
529 **Figure 6** Spatial distribution of the day-to-day changes in surface PM<sub>2.5</sub> (a–c), PM<sub>10</sub> (d–f), SO<sub>2</sub> (g–i), NO<sub>2</sub> (j–l), and CO (m–  
 530 o) concentrations following the three diurnal cycles within one day.



532

533 **Figure 7** Day-to-day changes in the PT vertical profiles at 20:00 BJT following the three identified diurnal cycles within one

534 day at four sounding stations. Chengdu (a–c), Yibin (d–f), Dazhou (g–i), and Chongqing (j–l).



535  
 536 **Figure 8** Spatial distribution of the day-to-day changes in LTS (a–c), PBLH (d–f), and WS (g–i) following the three  
 537 identified diurnal cycles within one day.

538

539